LIMNOLOGY and OCEANOGRAPHY

ASLO

Limnol. Oceanogr. 64, 2019, 2152–2160

doi: 10.1002/lno.11175

Observations of radiatively driven convection in a deep lake

Jay A. Austin *

Large Lakes Observatory and Department of Physics and Astronomy, University of Minnesota Duluth, Duluth, Minnesota

Abstract

Observations of radiatively driven convection in deep, ice-free Lake Superior from a set of moorings and an autonomous glider are used to characterize the spatial and temporal scales of the phenomenon. The moored observations show that instability builds at the surface on scales of hours, water near the bottom of the lake begins warming roughly 6 h after sunup, and the water column homogenizes a few hours after sundown. Glider observations suggest the existence of distinct convective chimneys, which carry warmed water to depth with horizontal scales on the order of tens of meters. Patches of photoquenched phytoplankton coincide with patches of anomalously warm water, providing a secondary tracer of water recently in the euphotic zone, and provide insight into the vertical development of convective chimneys. An analysis of the abundance of convective chimneys is used to estimate the lateral scale of convective cells, which appears to be on the order of 50 m.

Convective processes are a ubiquitous and important part of circulation and mixing in geophysical systems, including both limnological (Bouffard and Wüest 2018) and oceanographic (Marshall and Schott 1999). Radiatively driven convection (RDC) occurs when surface solar radiation heats near-surface water, which is below the temperature of maximum density (hereafter T_{MD}, 3.98°C for surface freshwater). It becomes denser as it warms, developing an unstable water column which undergoes convection. This process is distinct from most examples of convection in the oceanographic context, in which surface cooling drives densification of salt water. Surface cooling is typically associated with high winds, which drive large sensible and latent cooling, but also provide a significant surface input of turbulent kinetic energy (TKE). RDC provides a scenario in which to consider convective processes in the absence of wind-induced shear. In addition, RDC is distinct from convection driven by surface cooling in that the source of buoyancy is distributed over the euphotic layer rather than being applied at the surface, a distinction which is often referred to as the "ultimate" regime of thermal convection (Lepot et al. 2018).

Anecdotal observations of springtime, under-ice convection go back as far as Birge (1910) and Barnes (1910), who speculated that convective processes were to an extent responsible for the quick disappearance of ice on small lakes in the spring, as well as a number of papers detailing the appearance of ice cover in the spring (e.g., Woodcock 1965), in which regular cell-like structure appears in the melt pattern on shallow lakes. The first study to investigate the thermal structure of ice-covered lakes was undertaken by Farmer (1975), who placed instrumentation in Babine Lake (British Columbia), including thermistor chains and an electric bathythermograph. The focus of that work was primarily on the relative inefficiency of transforming convection-related kinetic energy to changes in potential energy as the mixed layer penetrated into deep stratification. RDC has been investigated more recently in ice-covered lakes, which are typically characterized by a thin boundary layer immediately below the ice, a convective layer which thickens over the season, and a quiescent, stratified layer below (Kirillin et al. 2012). Mironov et al. (2002) considered the phenomenon in a range of high-altitude lakes, as well as with large-eddy simulations, showing that the distributed nature of the radiative forcing was important to take into consideration in order to be consistent with classical scalings. Jonas et al. (2003*a*) examined the TKE structure and balance under the ice in relatively shallow (7 m) Lake Vendyurskoe, discerning details of the interaction between layers. Vertical velocities associated with the convective processes can create internal waves in the stratified waters below the convective layer (Bouffard et al. 2016). While most of these references address bulk response of the convective layer, focusing on vertical structure, convective process can have relatively short horizontal scales of variability (Forrest et al. 2008), which cannot be resolved with traditional point moorings. Impacts of RDC on biogeochemical processes have also been considered, including primary productivity (Kelley 1997; Vehmaa and Salonen 2009) and dissolved oxygen distributions (Yang et al. 2017). Recent work (Ulloa et al. 2018) has provided insights into the energy budget, showing that about 65% of the energy input through the radiative buoyancy flux is converted into changes in potential energy.

*Correspondence: jaustin@d.umn.edu

Several aspects distinguish Lake Superior's RDC season from lakes previously considered. In marked contrast to the lakes considered in previous literature, Lake Superior waters experience very little warming during periods of ice cover (Titze and Austin 2014). Ice does not start forming until there is a surface mixed layer with thickness approaching 100 m and temperatures on the order of 0.1°C, and this layer persists until ice is removed (Titze and Austin 2014). This is likely due to snow cover on the ice preventing significant levels of shortwave radiation from reaching the water below, given the high albedo of snow. For the open lake, it is likely that ice is advected away from a region, rather than melting locally, exposing sub-T_{MD} water to full surface heat and momentum fluxes in the absence of ice. This lack of ice during the RDC period has several implications: there is no boundary layer between the convective layer and overlying ice, the water experiences a range of wind-induced shear, and the heat (and hence buoyancy) flux is much greater than if there was ice present.

A second distinction has to do with the deep thermal structure. Immediately after the removal of ice, there is typically a deep layer of slightly warmer water, a feature common to smaller ice-covered lakes (Kirillin et al. 2012). In the case of Lake Superior, the cold surface and warm deep water are quickly mixed by vigorous spring storms, resulting in an isothermal water column (Titze and Austin 2014). At this stage, the RDC cycle dominates the vertical circulation until the onset of positive stratification once the surface waters reach T_{MD}. This convectively dominated period, the subject of this article, can last for 1–3 months depending on the initial heat content of the water column and the local water depth. This represents a significant fraction of the year, of which very little is known.

A final distinction is that Lake Superior is deep; with the exception of Farmer's (1975) work in Lake Babine (~ 200 m), most work on RDC in ice-covered lakes has occurred in relatively shallow lakes; deployment depths of recent work in Lake Vendyurskoe (10 m; Jonas et al. 2003*a*; Volkov et al. 2018), Pavilion Lake (~ 50 m; Forrest et al. 2008), and Lake Onega (28 m; Bouffard et al. 2016; Ulloa et al. 2018) are all relatively shallow compared to the deployment depths of 154–185 m considered here. This leads to the long duration of the RDC season in Lake Superior, but is also significant because there may be vertical scales upon which vertically descending plumes of warmed water eventually equilibrate with the ambient water. Both the moored and glider data suggest a different response below roughly 100 m than that observed in the top 100 m.

A set of opportunistic observations taken over the last several years as part of other projects provides us with the ability to characterize this process in a deep, ice-free lake. We limit the scope of this article to a study of the properties of the convective process. We will not consider thermobaric effects as the water column temperature nears the temperature of maximum density; nor will we consider the dynamics of thermal bars, both interesting, but distinct, springtime phenomena. We will focus on two sets of observations: Temperature observations from three moorings deployed in western Lake Superior in 2016–2017 (Fig. 1), and glider transects from central Lake Superior taken in 2013 (Fig. 1). The moored data provide high temporal resolution and moderate vertical resolution at distinct locations in the lake, providing insights into the temporal development of the convective process. In contrast, glider data provide insight into the horizontal structure of convective chimneys, a novel result. Convective chimneys of downwelling warmed water are shown to have horizontal scales of O(10 m), and the convective cells themselves have scales of O(50 m). It is worth noting that the moored and glider observations are not coincident with each other temporally or colocated spatially, and therefore direct quantitative comparisons are likely not justifiable. However, it is reasonable to expect that the same process is occurring broadly across the lake and is not a regional phenomenon, and as the goal of this article is to develop a characterization of the spatial and temporal scales of RDC in deep, ice-free lakes, it is useful to consider both mooring and glider data.

Methods

Three moorings were deployed in western Lake Superior on 17 and 18 May 2016 and recovered on 14 and 15 July 2017. These moorings are referred to as GM1, GM2, and WM (for "Grand Marais 1," "Grand Marais 2," and "Western Mooring," respectively), in water depths of 154 m, 168 m, and 185 m, respectively (Fig. 1). The WM site, which is the primary focus of the mooring analysis, is over 50 km offshore (both to the northwest and southeast) in a region of relatively featureless bathymetry. Each mooring had RBR-solo thermistors at depths of 10, 15, 20, 25, 30, 40, 50, 60, 81, and 100 m; GM1 had another thermistor at 150 m, GM2 had another at 160 m, and WM had two more thermistors at 150 and 180 m. Thermistors all recorded at 0.5 Hz and have a reported initial accuracy of

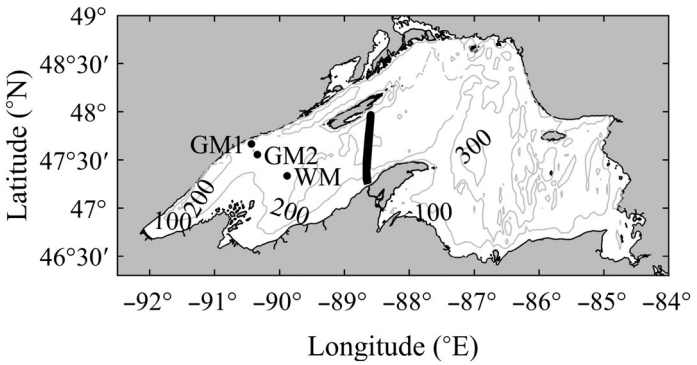

Fig. 1. Map of study site. 2016–2017 moorings located at GM1, GM2, and WM; 2013 glider transect extends from the Keweenaw Peninsula to Isle Royale and back. Depth contours in meters.

0.002°C and resolution of 0.00005°C. All thermistors on GM1 below 50 m failed before the 2017 RDC season. We will display in situ temperature; potential temperatures are within 0.001°C of in situ temperatures due to the very small values of the coefficient of thermal expansion near T_{MD}. Salinity is very low in Lake Superior, on the order of 50 μg L^{-1} (Chapra et al. 2012) and will be disregarded. In this article, we will focus our attention on WM during 2017; data from the other moorings are used to make the case that the response is similar at different locations.

Following Farmer (1975), performing a harmonic analysis on the individual thermistor temperature records allows the determination of the depth dependence of the magnitude of the diurnal signal, and the phase of the signal as it propagates through the water column. Specifically, we evaluate

$$P_\omega = \frac{1}{t_2 - t_1}\int_{t_1}^{t_2} T(t)e^{-j\omega t}dt \quad (1)$$

where $\omega = 2\pi(24h)^{-1}$, $[t_1, t_2]$ is a time interval equal to an integer number of days, and $T(t)$ is a time series of temperature measured at a given depth. The magnitude of the signal decreases with depth, as expected, and can be fit with an offset exponential of the form

$$|P_\omega(z)| = P_0 + P_1 e^{z/z_0} \quad (2)$$

where P_0 is an offset, P_1 the magnitude of the vertical structure, and z_0 is the e-folding depth.

A Teledyne Webb Research G1 autonomous underwater glider transected the central basin of Lake Superior in May 2013, before the onset of summer stratification in the open lake that year. The glider collected data on downcasts only. Glider dive angle is fixed at 26°, so that the horizontal to vertical glide ratio is approximately 2:1. Dive depth is capped at 150 m, so that the spacing between adjacent dives is approximately 600 m. Along the glide path, the glider collected data on water temperature, conductivity, chlorophyll *a* (Chl *a*) fluorescence, colored dissolved organic matter fluorescence, and backscatter at a rate of approximately 1 Hz. The temperature sensor has an initial accuracy of 0.002°C and a resolution of 0.001°C. Further details of glider operation can be found in Austin (2013).

Results

Moored observations

At WM in 2017, temperature in the water column (Fig. 2) is homogeneous starting around 05 May, when the last of the deep warm water is mixed with the cold surface waters above. At this stage, the water column heats up at a rate of approximately 0.025°C d^{-1}, which, neglecting advective effects, corresponds to a surface heating rate of 220 Wm^{-2} for a depth of 185 m, consistent with surface heat flux climatology (Lofgren and Zhu 2000). As these observations were made for reasons other than to study RDC, direct observations of individual terms of the surface heat flux are not available. Whole water column temperature differences are on the order of 0.1°C during the day, but it should be noted that the shallowest measurement is at 10 m, so any variability in the top 10 m (where it might be expected to be largest) is being neglected. This continues until the end of June, at which point deep water reaches the T_{MD} at the bottom (approximately 3.6°C for 185 m), and the lake ceases to fully homogenize at night. Soon thereafter, the surface reaches T_{MD} for surface water, and the lake begins to stratify. The most distinct feature of the period prior to stratification is a series of strong daily spikes in near-surface temperatures, and a subsequent collapse at night to isothermal conditions. From a close-up of a 3-d period (Fig. 3A,B), it is clear that the warming is sporadic, with events that start at the surface and last on the order of hours, interspersed with significant homogenization events. At night, the water column becomes isothermal before local midnight.

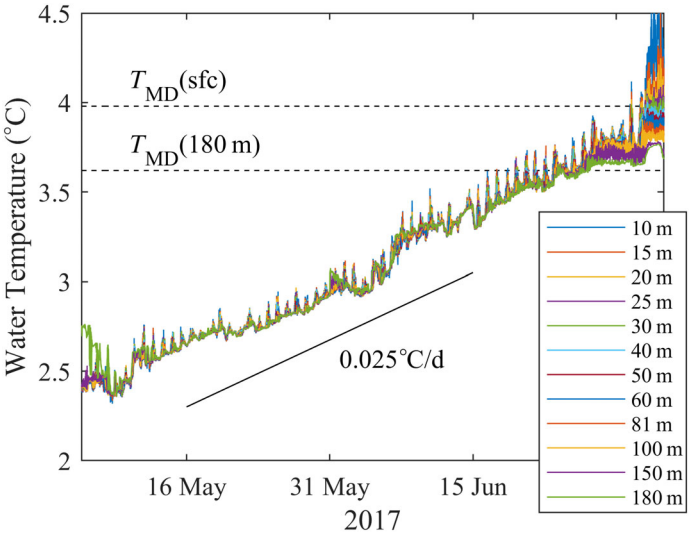

Fig. 2. Temperature at WM in 2017 at 12 different depths. Due to the nearly isothermal nature of the water column prior to June, the individual temperature records are difficult to discern.

An average of temperature anomalies between 20 May and 20 June (Fig. 4A,B) provides a composite view of the development of the water column over the course of a day. Because this is an averaged view, individual convective events are smoothed over. Warming begins at the surface at 6 h past local midnight, corresponding to sunup, and surface temperatures reach a peak for a few hours past local noon. The surface cools for the next several hours, as it homogenizes with deeper waters, and the water column temperature difference is small by midnight. At the bottom, warming begins around local noon, and continues until midnight, at which point the water column is homogenous. The onset of warming at the bottom at noon suggests that parcels of water must have average vertical velocities on the order of $\frac{185\,\mathrm{m}}{6\,\mathrm{h}} \approx 0.9\,\mathrm{cm\,s^{-1}}$ in order to

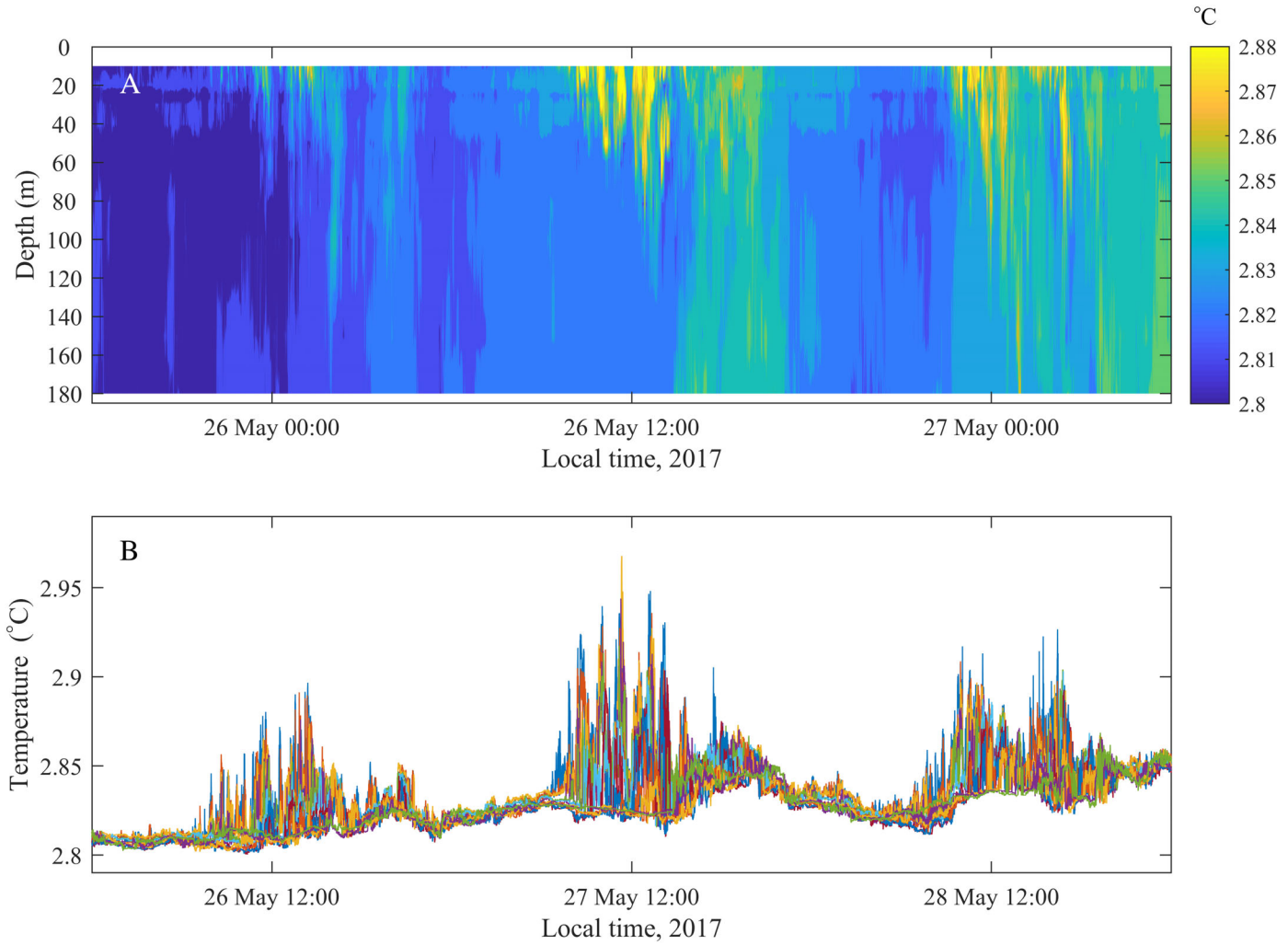

Fig. 3. Close-up of 26–29 May 2017 temperature at WM. (**A**) Contour plot. (**B**) Line plot of same data. Colors are the same as in Fig. 2. Time is local (CDT).

deliver warmed water to the bottom within 6 h. This compares favorably to the vertical velocity scale of convective plumes (also known as the Deardorff velocity scale), which following Deardorff (1970) is given by $v_p \approx (-Bh)^{1/3}$, where B is the buoyancy flux ($m^2\ s^{-3}$) and h is the depth of the mixed layer. In addition to the diurnal cycle in buoyancy flux, the buoyancy flux will decrease as the water warms since the coefficient of thermal expansivity goes to zero as the temperature approaches T_{MD}. As the water column is isothermal, we take mixed layer depth to be the local water depth. For the value of the thermal expansivity at 2.5°C of $\alpha = 2.5 \times 10^{-5} K^{-1}$ and a surface heat flux of 200 Wm^{-2}, the vertical velocity scale is $v_p \approx 1.2$ cm s^{-1}, consistent in magnitude with the observed onset of warming at the bottom of the lake. As the lake warms past 2.5°C, the coefficient of thermal expansivity decreases as would the vertical velocity scale. In addition, the time scale of convective decay, given by

$$\tau \approx C\left(h^2/B\right)^{1/3}$$

where C is an empirically determined constant, taken here to be 0.6 (Lombardo and Gregg 1989; Kelley 1997), yields a relaxation time scale on the order of 2 h, consistent with the water column fully adjusting before local midnight.

For the 2016 data, a harmonic analysis was performed over a 21-d interval from 19 May to 10 June, and in 2017, over a 31-d period from 12 May to 12 June. These dates were chosen to avoid both the last vestiges of deep winter stratification and the onset of summer stratification, so that at all sites, convection took place over the entire water column. Offsets are typically on the order of 0.05–0.1°C, and the e-folding scale is on the order of 25 m (Table 1). From Conductivity-temperature-depth casts (e.g., Sterner 2010) taken in the open waters of Lake Superior (but not coincidentally with this data), the e-folding scale for

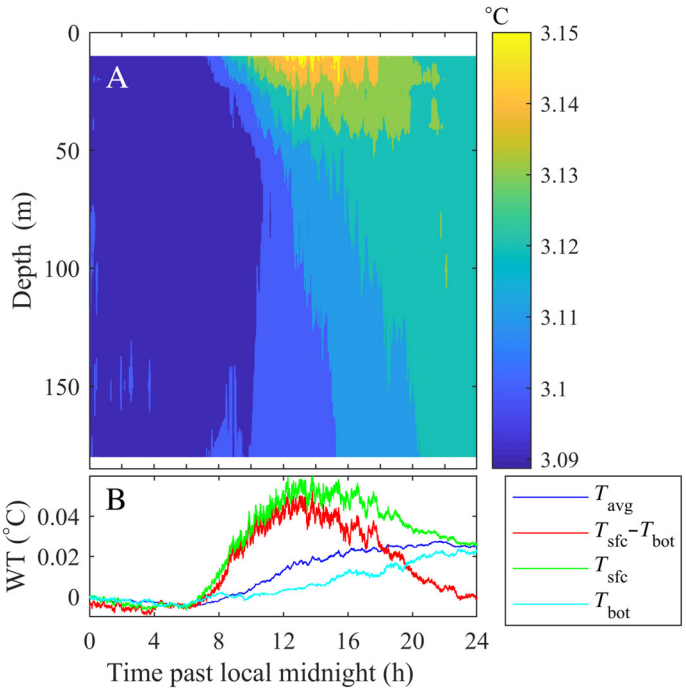

Fig. 4. (**A**) Diurnal composite plot of 15 May–15 June at WM in 2017. (**B**) Summary statistics of diurnal cycle. Blue: water column average temperature; Red: surface to bottom difference; Green: surface temperature; Light blue: bottom temperature.

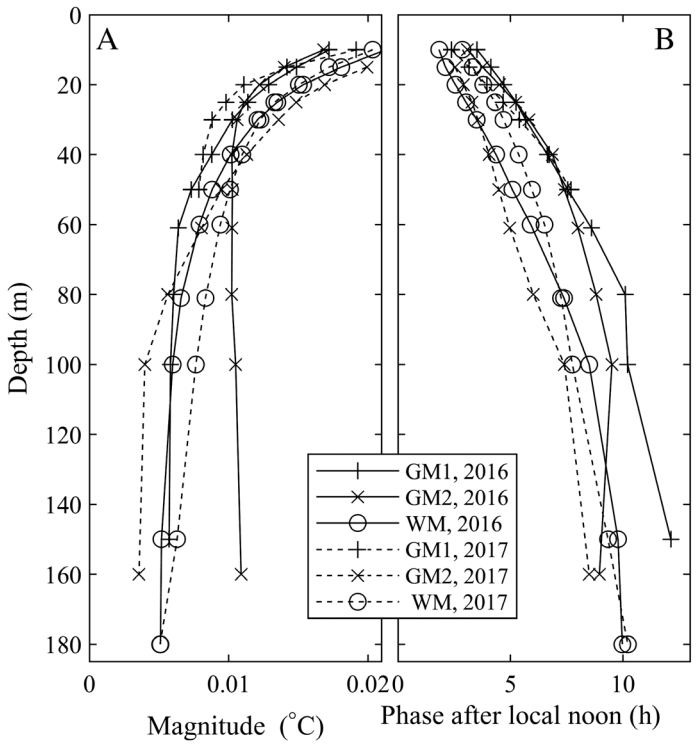

Fig. 5. Harmonic analysis of data from three moorings in the RDC seasons of 2016 and 2017. (**A**) Magnitude of signal, |P|. (**B**) Phase of signal relative to the solar diurnal cycle. A phase lag of 0 h represents a diurnal temperature maximum around local noon.

shortwave radiation tends to be on the order of 10 m, significantly smaller than the scale of this process. An extrapolation to the surface implies that the magnitude of the signal at the surface should be roughly 1.6 times greater than that at 10 m.

The phase propagation of the signal (Fig. 5B) is typically slower in the top 80–100 m and is scattered around an equivalent downward propagation speed of 4 mm s^{-1} (Table 2). This is faster, but of the same order estimated by Farmer (1975) for a deployment on Babine Lake, for which he found a downward propagation speed of 2.2 mm s^{-1}. Below 80 m, the phase of the response appears to be relatively uniform in depth, in some cases suggesting the lower portion of the lake responds almost uniformly, so that different processes may dominate in the upper and lower portions of the water column.

Glider observations

A glider transect during May 2013 took place prior to the onset of stratification of the lake (although shallow coastal areas sampled on this transect had begun to stratify). The data shown represent a full round trip, from the Keweenaw Peninsula at the southern extent of the transect to Isle Royale in the north and back; here it is plotted as a function of local time. The temperature field is displayed (Fig. 6A), where each individual profile has been vertically demeaned, in order to emphasize the vertical structure of the profiles. During daylight hours, there are frequent "hot spots," showing patches of water which are O(0.1°C) warmer than the rest of the water column (the near-coastal waters shown at the beginning and end of the transect have already stratified). These patches tend to be concentrated toward the surface, but can be observed as deep as 100 m in places.

In addition, the Chl *a* fluorescence signal (Fig. 6B) appears to be dominated by large parabolic regions at the surface where the fluorescence signal becomes small. Rather than indicating regions of low chlorophyll content, these represent regions of fluorescence quenching, where bright sunlight has overwhelmed the photosystems of photosynthetic organisms, drastically reducing their ability to fluoresce (Falkowski and Kiefer 1985; Oliver et al. 2003). The roughly parabolic shape of these regions is due to the diurnal variability of solar radiation and hence the depth of the

Table 1. Vertical scale of harmonic analysis (in meters).

	2016	2017
GM1	22	—
GM2	7.7	36
WM	25	29

Table 2. Phase propagation speed (mm s^{-1}).

	2016	2017
GM1	3.5	—
GM2	3.9	4.4
WM	3.6	5.1

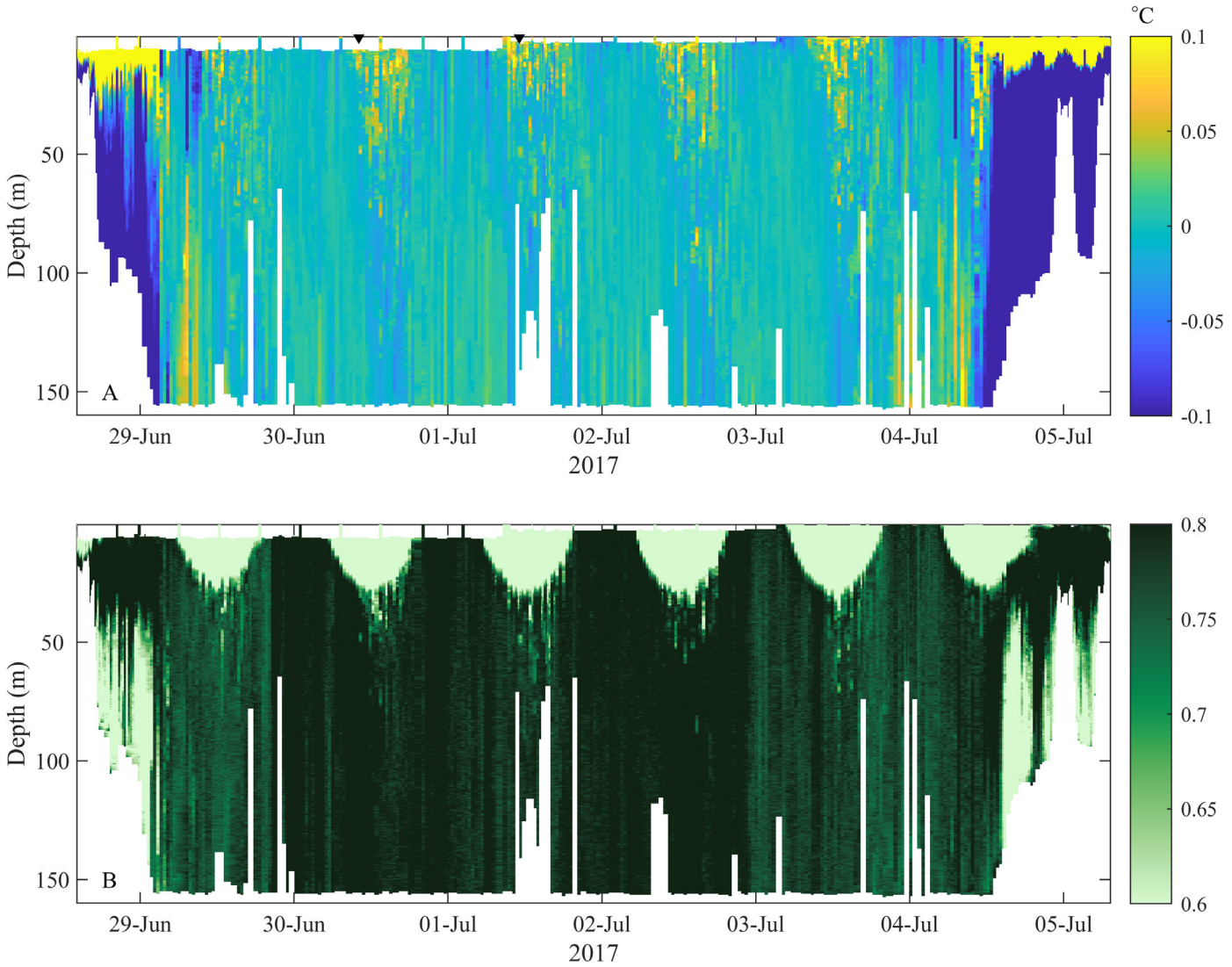

Fig. 6. Glider transects in 2013, plotted as a function of time. (**A**) Temperature. (**B**) Chl *a* fluorescence. Black triangles mark the timing of profiles in Fig. 7. The phase of the shortwave signal is apparent from the fluorescence transect. The anomalous regions are the light patches below about 30 m.

euphotic zone. Because the Chl *a* fluorescence signal is, in this case, dominated by this quenching effect rather than variability in chlorophyll concentration, we do not include units on the plots, which could be misleading. Given that the recovery time of phytoplankton to quenching is on the order of tens of minutes to a few hours (Oliver et al. 2003), this provides a convenient tracer of water that has recently been exposed to high levels of shortwave radiation. Like the temperature field, the signal below these daytime regions displays noise with small patches of anomalously low fluorescence appearing over a range of depths. Aside from the surface photoquenched region and the small anomalous patches, Chl *a* fluorescence is relatively vertically uniform, although there is significant along-track variability.

An analysis of temperature anomalies and fluorescence anomalies show that they are coincident. As an example, two individual profiles (Fig. 7A,B) plotted as traditional vertical profiles show spikes in temperature that correspond to regions of low fluorescence. An analysis of 250 profiles made during this deployment identified 75 negative anomaly events in the Chl *a* fluorescence field. To identify anomalous regions in fluorescence, the upper 30 m is disregarded since it is directly photoquenched. The vertical mean of the remaining data is removed for each individual profile to emphasize variability within a profile rather than between-profile variability. Anomalous regions were identified as local minima which exceeded a threshold of more than 3 SDs below the mean value and spanned at least 5 m in the vertical. For each of these anomalies, the corresponding temperature anomaly was determined as the departure of the temperature at the same depth from the vertical mean. Each (save one) of the Chl *a* fluorescence anomalies corresponded to a positive temperature anomaly (Fig. 8), suggesting that theses anomalies represent water which has recently been at or near the surface. There is a

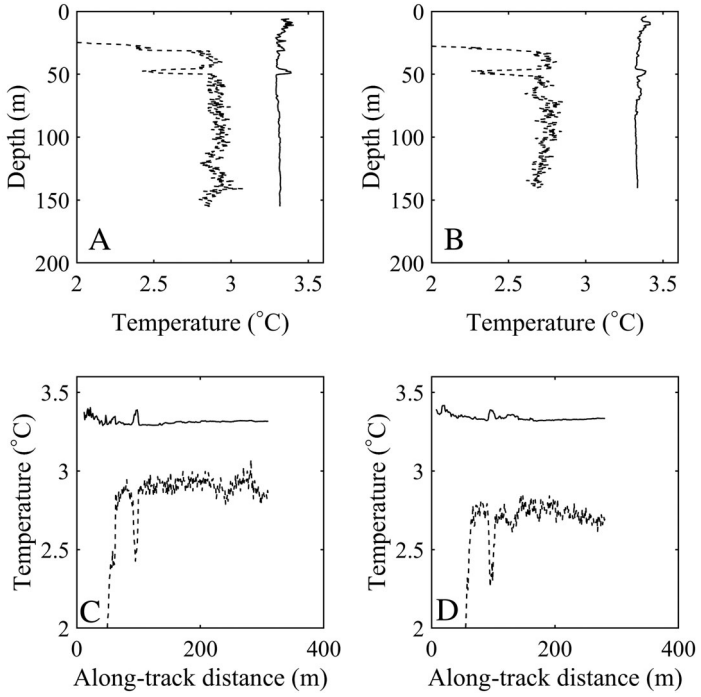

Fig. 7. Individual glider profiles from (**A**, **C**) 30 June and (**B**, **D**) 01 July, displayed as vertical profiles and as along-track data. Solid line is temperature and dashed is Chl *a* fluorescence.

noisy but discernible correspondence between their intensities, with large negative Chl *a* fluorescence anomalies corresponding to larger positive temperature anomalies. Part of the reason that the relationship between these anomalies is noisy is that as a parcel of warm, Chl *a* fluorescence-depleted water descends, its waters mix with the ambient water around it, reducing the size of both the temperature and Chl *a* fluorescence anomaly. At the same time, the Chl *a* photosystem is recovering on time scales of tens of minutes to hours (Oliver et al. 2003). Therefore, we would expect anomalies observed at greater depths (and hence older) to have smaller Chl *a* fluorescence anomalies relative to temperature than shallow ones. In fact (Fig. 8), anomalies detected deeper than 60 m (x's) have smaller Chl *a* anomalies relative to their corresponding temperature anomalies than shallow ones (dots). Finally, the anomalies occurred almost exclusively during daylight hours (Fig. 9A). The intensity of the Chl *a* fluorescence anomalies does not appear to depend on the time of day (Fig. 9A); however, the depth at which they are observed does appear to increase as the day progresses (Fig. 9B).

Glider data are traditionally interpreted as a collection of vertical profiles; this is a reasonable interpretation in regions where horizontal variability is small compared to vertical variability, which is typically the case. However, it is unlikely from a dynamical standpoint that the glider, in passing through anomalous regions, is passing through horizontal layers of anomalously warm, low Chl *a* fluorescence water. In addition, anomalies observed in each profile do not appear in previous or subsequent profiles, further suggesting that these are not horizontal structures. In addition, the vertical coherence suggested by the moored data suggests that the anomalies are not isolated boluses of water. A better interpretation of the data is that the glider, with a relatively gentle dive angle of 26°, is passing through downwelling vertical chimneys of convection cells (Fig. 7C,D) (an alternate hypothesis is that the downwelling warm water is organized in a two-dimensional "sheet," as suggested by the modeling work of Mironov et al. 2001). The chimneys appear to have a horizontal scale on the order of 10 m, although this is a lower bound since the glider is not necessarily traveling through the center of the chimneys it encounters. In addition, the glider data suggest that the boundary between the relatively warm, downwelled water within the chimney and the ambient, slowly upwelling water is very sharp, typically on the order of a meter or less.

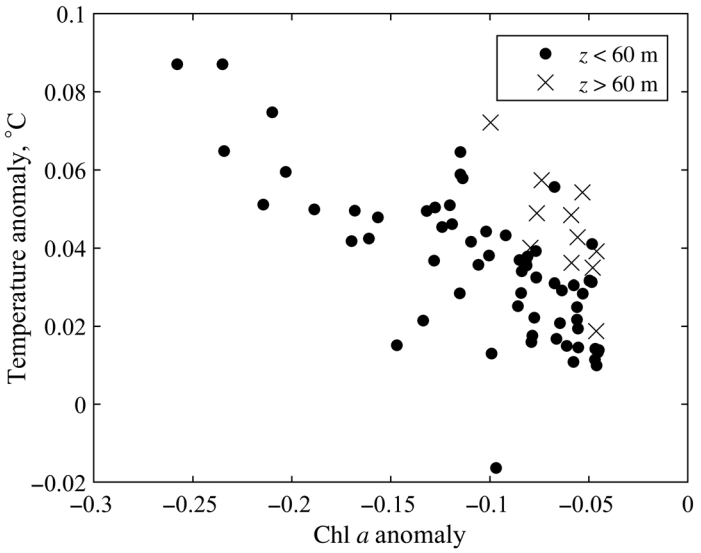

Fig. 8. Temperature anomaly as a function of Chl *a* fluorescence anomaly for 75 identified Chl *a* anomalies.

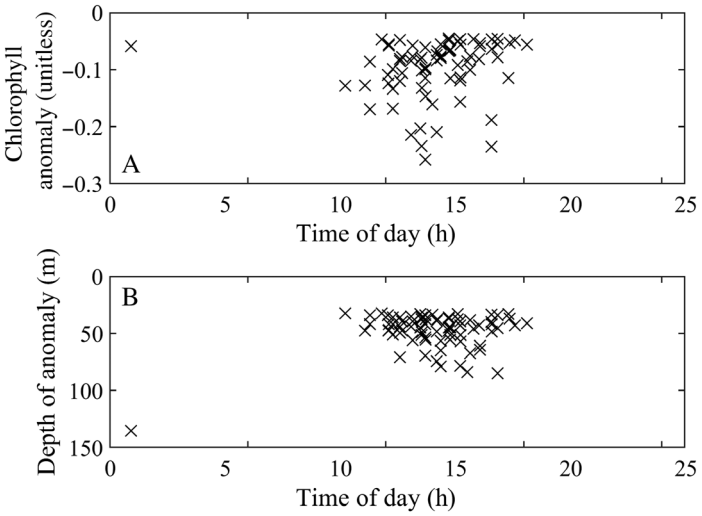

Fig. 9. (**A**) Intensity of Chl *a* fluorescence anomaly as a function of local time (hours past midnight). (**B**) Observed depth of anomaly as a function of local time.

This alternate interpretation of the glider data along with a measure of the abundance of anomalous events allows us to make an order of magnitude estimate of the spatial scales of convective cells. The Chl *a* signal is a less noisy signal with which to discern anomalous regions. Since it decays as water descends in a chimney, we look at the relative abundance of anomalous water in the 30–80 m range during daylight hours. Under these conditions, the glider was inside a region of high temperature, low Chl *a* fluorescence water about 5% of the time. In addition, we can use the depth range of an anomalous event and the dive angle to estimate that the average horizontal span of a region was on the order of 10 m (e.g., Fig. 7C,D). A typical chimney is therefore going to have a cross-sectional area on the order of $(10\ \text{m})^2 \sim 100\ \text{m}^2$. If convective cells and their respective chimneys are randomly distributed, and chimneys take up about 5% of the total area, we should expect that the cells take up an area approximately 20 times that of the chimneys. Therefore, the area of a cell is on the order of $20 \times (100\ \text{m}^2) \sim 2000\ \text{m}^2$, which yields a length scale of the convective cells of roughly 50 m. The result that the downwelling plume is much smaller than the compensating upwelling is not consistent with the numerical results of Sander et al. (2000) or the fall convection season observational results of Jonas et al. (2003*b*), who both estimated that the downwelling plume and the upwelling return flow are roughly equal in area. However, it is at least qualitatively consistent with Mironov et al. (2001), whose large eddy simulation modeling suggested the downwelling regions are "more localized" that the upwelling ambient water.

Discussion and conclusions

The existence of variability on very short horizontal scales raises the issue that most of our current observational techniques, while providing high resolution in the vertical dimension, do a poor job of resolving lateral variability. For instance, when moored data are considered (as in this article), a tacit assumption is made that it is in some sense representative of conditions in a lateral region around it. In the case of convective chimneys with scales likely on the order of tens of meters, this assumption does not hold, and moored data become more difficult to correctly interpret. In this case, it is difficult to know at any instant whether the mooring is in a chimney or in the ambient water. What we end up observing is more likely a statistical reflection of how the background state is modified over time by the convective behavior. It must be kept in mind then that the moored data do not show the whole picture, due to the intrinsically three-dimensional character of this process.

Two techniques do produce high lateral resolution data: remote sensing and ship underway systems. However, typical remote sensing platforms for sea surface temperature, such as Advanced Very High Resolution Radiometer, have lateral resolution on the order of 1 km (http://noaasis.noaa.gov/NOAASIS/ml/avhrr.html, accessed May 2018), too coarse for the current purpose. An examination of 3 yr of underway data from the Research Vessel Blue Heron does show more high frequency noise, on the order of 0.1°C, in the temperature signal during the day, but the horizontal resolution of the signal while underway is on the order of 10 m and may not be resolving individual convection cells. Research planned for the next field season will include the deployment of a large, horizontal mooring, like that discussed in Grosenbaugh (2002), consisting of two moorings attached by an instrumented horizontal "head-line." Along with careful characterization of the surface heat flux, acoustic current Doppler profiler measurements, and focused glider deployments, this will allow us to discern more reliably the horizontal scales of this phenomenon.

This article is a first observational study at RDC in deep, ice-free Lake Superior. Moored data provided evidence of intermittent vertically coherent plume-like structures during daylight hours, with vertical e-folding scales on the order of 20 m, significantly in excess of the e-folding scale of shortwave radiation. Temperature anomalies near the surface are on the order of 0.1°C and decrease with depth. Warming begins at the bottom of the lake roughly 6 h after sunup, suggesting the presence of vertical velocities on the order of 1 cm s^{-1}, consistent with classical scalings of vertical convective velocities. The water column homogenizes a few hours after sundown, also consistent with classical scalings of convective decay scales. Glider observations show distinct anomalous regions in both temperature and in Chl *a* fluorescence, which is a result of surface photoquenching. These regions are coincident, implying that they represent water recently at or near the surface. We interpret these regions to be vertical chimney-like structures that the glider is passing through horizontally. This interpretation and the abundance of these anomalous regions allow some estimates of chimney lateral scale and, ultimately, the lateral scale of convective cells themselves, which appear to be on the order of 50 m.

References

Austin, J. A. 2013. The potential for Autonomous Underwater Gliders in large lake research. J. Great Lakes Res. **39**: 8–13. doi:10.1016/j.jglr.2013.01.004

Barnes, H. T. 1910. On the apparent sinking of surface ice in lakes. Science **31**: 856–857. doi:10.1126/science.31.805.856-a

Birge, E. A. 1910. The apparent sinking of ice in lakes. Science **32**: 81–82. doi:10.1126/science.32.811.81

Bouffard, D., R. E. Zdorovennov, G. E. Zdorovennova, N. Pasche, A. Wüest, and A. Y. Terzhevik. 2016. Ice-covered Lake Onega: Effects of radiation on convection and internal waves. Hydrobiologia **780**: 21–36. doi:10.1007/s10750-016-2915-3

Bouffard, D., and A. Wüest. 2018. Convection in lakes. Annu. Rev. Fluid Mech. **51**: 189–215. doi:10.1146/annurev-fluid-010518-040506

Chapra, S. C., A. Dove, and G. J. Warren. 2012. Long-term trends of Great Lakes major ion chemistry. J. Great Lakes Res. **38**: 550–560. doi:10.1016/j.jglr.2012.06.010

Deardorff, J. W. 1970. Convective velocity and temperature scales for the unstable planetary boundary layer and for

Rayleigh convection. J. Atmos. Sci. **27**: 1211–1213. doi:10.1175/1520-0469(1970)027<1211:CVATSF>2.0.CO;2

Falkowski, P., and D. A. Kiefer. 1985. Chlorophyll *a* fluorescence in phytoplankton: Relationship to photosynthesis and biomass. J. Plankton Res. **7**: 715–731. doi:10.1093/plankt/7.5.715

Farmer, D. M. 1975. Penetrative convection in the absence of mean shear. Q. J. R. Meteorol. Soc. **101**: 869–891. doi:10.1002/qj. 49710143011

Forrest, A. L., B. E. Laval, R. Pieters, and D. S. S. Lim. 2008. Convectively driven transport in temperate lakes. Limnol. Oceanogr. **53**: 2321–2332. doi:10.4319/lo.2008.53.5_part_2.2321

Grosenbaugh, M., S. Anderson, R. Trask, J. Gobat, W. Paul, B. Butman, and R. Weller. 2002. Design and performance of a horizontal mooring for upper-ocean research. J. Atmos. Ocean Technol. **19**: 1376–1389. doi:10.1175/1520-0426(2002)019<1376:DAPOAH>2.0.CO;2

Jonas, T., A. Y. Terzhevik, D. V. Mironov, and A. Wüest. 2003*a*. Radiatively driven convection in an ice-covered lake investigated by using temperature microstructure technique. J. Geophys. Res. **108**: 14-1–14-18. doi:10.1029/2002JC001316

Jonas, T., A. Stips, W. Eugster, and A. Wüest. 2003*b*. Observations of a quasi shear-free lacustrine convective boundary layer: Stratification and its implications on turbulence. J. Geophys. Res. **108**: 26-1–26-15. doi:10.1029/2002JC001440

Kelley, D. E. 1997. Convection in ice-covered lakes: Effects on algal suspension. J. Plankton Res. **19**: 1859–1880. doi:10.1093/plankt/19.12.1859

Kirillin, G., and others. 2012. Physics of seasonally ice-covered lakes: A review. Aquat. Sci. **74**: 659–682. doi:10.1007/s00027-012-0279-y

Lepot, S., S. Aumaitre, and B. Gallet. 2018. Radiative heating achieves the ultimate regime of thermal convection. Proc. Nat. Acad. Sci. USA **115**: 8937–8941. doi:10.1073/pnas.1806823115

Lofgren, B., and Y. Zhu. 2000. Surface energy fluxes on the Great Lakes based on satellite-observed surface temperatures 1992 to 1995. J. Great Lakes Res. **26**: 305–314. doi:10.1016/S0380-1330(00)70694-0

Lombardo, C. P., and M. C. Gregg. 1989. Similarity scaling of viscous and thermal dissipation in a convecting surface boundary layer. J. Geophys. Res. **22**: 1821–1828. doi:10.1029/JC094iC05p06273

Marshall, J., and F. Schott. 1999. Open-ocean convection: Observations, theory, and models. Rev. Geophys. **37**: 1–64. doi:10.1029/98RG02739

Mironov, D., A. Terzhevik, G. Kirillin, T. Jonas, J. Malm, and D. Farmer. 2002. Radiatively driven convection in ice-covered lakes: Observations, scaling, and a mixed-layer model. J. Geophys. Res. **107**: 3032. doi:10.1029/2001JC000892

Mironov, D. V., S. D. Danilov, and D. J. Olbers. 2001. Large eddy simulation of radiatively driven convection in ice covered lakes, p. 71–75. *In* X. Casamitjana [ed.], Proceedings of the Sixth Workshop on Physical Processes in Natural Waters, Girona. Univ. of Girona.

Oliver, R. L., J. Whittington, Z. Lorenz, and I. T. Webster. 2003. The influence of vertical mixing on the photoinhibition of variable chlorophyll a fluorescence and its inclusion in a model of phytoplankton photosynthesis. J. Plankton Res. **25**: 1107–1129. doi:10.1093/plankt/25.9.1107

Sander, J. A., A. Simon, T. Jonas, and A. Wüest. 2000. Surface turbulence in natural waters: A comparison of large eddy simulations with microstructure observations. J. Geophys. Res. Oceans **105**: 1195–1207. doi:10.1029/1999JC900266

Sterner, R. W. 2010. *In situ*-measured primary production in Lake Superior. J. Great Lakes Res. **36**: 139–149. doi:10.1016/j.jglr.2009.12.007

Titze, D. J., and J. Austin. 2014. Winter thermal structure of Lake Superior. Limnol. Oceanogr. **59**: 1336–1348. doi:10.4319/lo.2014.59.4.1336

Ulloa, H. N., A. Wüest, and D. Bouffard. 2018. Mechanical energy budget and mixing efficiency for a radiatively heated ice-covered waterbody. J. Fluid Mech. **852**: R1. doi:10.1017/jfm.2018.587

Vehmaa, A., and K. Salonen. 2009. Development of phytoplankton in Lake Paajarvi (Finland) during under-ice convective mixing period. Aquat. Ecol. **43**: 693–705. doi:10.1007/s10452-009-9273-4

Volkov, S., S. Bogdanov, R. Zdorovennov, G. Zdorovennova, A. Terzhevik, N. Palshin, D. Bouffard, and G. Kirillin. 2018. Fine scale structure of convective mixed layer in ice-covered lake. Environ. Fluid Mech. doi:10.1007/s10652-018-9652-2

Woodcock, A. H. 1965. Melt patterns in ice over shallow waters. Limnol. Oceanogr. **10**: R290–R297. doi:10.4319/lo.1965.10.suppl2.r290

Yang, B., J. Young, L. Brown, and M. Wells. 2017. High-frequency observations of temperature and dissolved oxygen reveal under-ice convection in a large lake. Geophys. Res. Lett. **44**: 12218–12226. doi:10.1002/2017GL075373

Acknowledgements

The author would like to acknowledge enlightening discussions with Stefan Llewellyn-Smith, Alberto Scotti, and Samuel Kelly conducted during the preparation of this manuscript, as well as technician Daniel Titze and the deck crew of the R/V *Blue Heron*, who participated in the collection of mooring data. Glider operations were supported by the US IOOS office for the development of the Great Lakes Observing System. Samuel Kelly provided data from moorings GM1 and GM2 with support from NSF-OCE-1635560. The author was supported under NSF-OCE-1829895 during the preparation of this manuscript.

Conflict of Interest

None declared.

Submitted 18 June 2018
Revised 01 February 2019 and 15 March 2019
Accepted 22 March 2019

Associate editor: Francisco Rueda